Mol Neurobiol (2012) 45:247–257
DOI 10.1007/s12035-012-8248-y

# Lipofuscin Accumulation and Gene Expression in Different Tissues of *mnd* Mice

**Giovanna Traina · Paolo Bigini · Giuseppe Federighi · Leopoldo Sitia · Gabriela Paroni · Fabio Fiordaliso · Monica Salio · Caterina Bendotti · Marcello Brunelli**

Received: 24 October 2011 / Accepted: 15 February 2012 / Published online: 8 March 2012


**Abstract** Neuronal ceroid lipofuscinoses (NCLs) are a group of lysosomal storage diseases characterized by neurological impairment and blindness. NCLs are almost always due to single mutations in different genes (CLN1–CLN8). Ubiquitous accumulation of undigested material and of a hydrophobic inner mitochondrial membrane protein, the subunit *c* of mitochondrial ATP synthase, has been described. Although protein mutation(s) in the endoplasmic reticulum–lysosomes axis can modify the trafficking and the recycling of different molecules, one of the upstream targets in these diseases may be represented by the balance of gene expression. To understand if and how neurons modify the levels of important genes during the first phases of the disease, it is important to characterize the mechanisms of neurodegeneration. Due to the impossibility of performing this analysis in humans, alternative models of investigation are required. In this study, a mouse model of human NCL8, the *mnd* mouse has been employed. The *mnd* mice recapitulate many clinical and histopathological features described in NCL8 patients. In this study, we found an altered expression of different genes in both central and peripheral organs associated with lipopigment accumulation. This is a preliminary approach, which could also be of interest in providing new diagnostic tools for NCLs.

**Keywords** *mnd* mice · Neuronal ceroid lipofuscinosis · Gene expression · Lipofuscin accumulation · Peripheral markers

**Abbreviations**

| | |
|---|---|
| NCL | Neuronal ceroid lipofuscinosis |
| SSH | Suppression subtractive hybridization |
| MS | Multiple sclerosis |
| MBP | Myelin basic protein |

## Introduction

Neuronal ceroid lipofuscinoses (NCLs) are a group of inherited, neurodegenerative, lysosomal-storage disorders characterized by the accumulation of autofluorescent material in many tissues and by progressive cognitive and motor deterioration, seizures, and early death. Phenotypes have been characterized by age of onset and order of appearance of the clinical features [1]. NCLs are classified in eight forms (NCL1-NCL8) associated with specific mutations in different genes belonging to the *CLN* family [2]. Mutations in the CLN8 gene, encoding an endoplasmic reticulum (ER) transmembrane protein of unknown function, underlie NCL phenotypes in humans and mice. The human phenotype is characterized by epilepsy, progressive psychomotor deterioration, and visual loss, whereas motor neuron degeneration (*mnd*) mice with a CLN8 mutation show progressive motor neuron dysfunction and retinal degeneration. Although this CLN8 mutation differs from the human type [3], *mnd* mice

G. Traina and P. Bigini equally contributed to this work.

G. Traina (✉)
Department of Economics and Food Sciences,
University of Perugia,
Via San Costanzo,
06126 Perugia, Italy
e-mail: traina@unipg.it

P. Bigini · L. Sitia · G. Paroni · F. Fiordaliso · M. Salio · C. Bendotti
Mario Negri Institute for Pharmacological Research,
Milan, Italy

G. Federighi · M. Brunelli
Department of Biology, Unit of General Physiology,
University of Pisa,
Pisa, Italy

share several clinical and histopathological features with the human pathology. *mnd* mice exhibit early degeneration of retinal cells leading to blindness within 1–2 months of life, with accumulation of autofluorescent material, lipoperoxidation, caspase-dependent apoptosis, and reactive gliosis in all retinal layers [4, 5]. In addition, *mnd* mice exhibit mitochondria-degenerating agglomerates of mitochondrial ATP synthase subunit c [6, 7] and mitochondrial energy failure [8]. We previously showed that chronic treatment with acetyl-l-carnitine (ALC) fully restored the mitochondrial enzyme activities and slowed down the progression of the symptoms in *mnd* mice. Very interestingly, using the suppression subtractive hybridization method to search for differentially expressed genes, we observed that ALC treatment significantly modulated the expression of the following three genes: (1) lysosomal $H^+$/ATPase, V1 D gene; (2) ATP synthase lipid-binding protein, subunit c gene; and (3) myelin basic protein (MBP) gene, in the brain of healthy rats [9–11].

The present study was therefore aimed at: (1) evaluating whether the expression of these three ALC "responder" genes was actually altered in *mnd* mice before a clear spread of neurological disorders; (2) if these changes were associated with the accumulation of lipofuscin; and (3) if there was a feature common to all affected regions (brain, spinal cord, and eyes). Since CLN8 mutations leading to important alterations in peripheral cells occur ubiquitously in both humans and mice, our analysis was extended to the liver. This comparative analysis was aimed at evaluating whether the neurons develop specific alterations or whether they share with other cells the main common response mechanisms to *clns* mutation(s). Our findings may represent an original attempt to find out whether peripheral biomarkers are also reliable for neuronal defects.

## Materials and Methods

### Animals

Procedures involving animals and their care were conducted in conformity with the institutional guidelines that are in compliance with national (D.L. no. 116, G.U. suppl. 40, 18 February 1992, circular no. 8, G.U. 14 July 1994) and international laws and policies (EEC Council Directive 86/609, OJ L 358, 1, December 12, 1987). All efforts were made to minimize animal distress and to use only the number of animals necessary to produce reliable results. Homozygous mutants/*mnd* female mice (B6KB2) were originally obtained from Jackson Laboratories (Bar Harbor, ME, USA). Both *mnd* and age-matched wild-type (WT) control mice with the same background (C57Bl6J) were then bred and maintained at Harlan Italy (Correzzana D'Adda, Milan, Italy). Mice were maintained at a temperature of 21±1°C and relative humidity of 55±10% with 12 h light/dark cycle. Food (standard pellets) and water were supplied ad libitum.

### Histological Evaluation of Autofluorescent Material

Five 10-week-old *mnd* female mice and the same number of age-matched wild-type (WT) mice were employed for the evaluation of the anatomical and histological distribution of lipopigment material. To ensure optimal quality for histological observation the mice were transcardially perfused [4% paraformaldehyde (*w*/*v*) in 0.1 M phosphate-buffered saline] under deep anesthesia with equithesin (1% vol/vol phenobarbital and 4% vol/vol chloral hydrate) 30 μl/10 g i.p.). The following steps were carried as previously described [12]. For each animal, the following organs were selected: Brain, lung, liver, spleen, kidneys, heart, and hind-leg muscles. Fifteen-micrometer-thick cryostatic sections obtained from the different tissues were collected and mounted on polylisined glass slides. By excluding brain and spinal cord, the analysis was carried out by visualizing at least ten sections for each single sample (representative of the whole organ) with an optical epifluorescent microscope (Olympus BX51). Images were acquired by an Olympus Camedia C-5060 digital compact camera and analyzed by the Olympus DPSoft software.

The evaluation of autofluorescent material in the central nervous system (CNS) was carried out by serially sectioning brains of both mnd and WT mice by either coronal ($n$=3) or sagittal ($n$=2) plane. Due to the ubiquitous presence of autofluorescent materials in neurons of *mnd* mice, every tenth serial section (first section, 11th section, 21st section, and so on) was collected. For the examination of autofluorescent material at the spinal cord level coronal sections for both *mnd* ($n$=3) and WT mice ($n$=3) were exclusively considered. Similarly to peripheral organs, brain and spinal sections were first captured by epifluorescent microscope (488 nm of wavelength). To verify if the signal produced by autofluorescent material was detectable at multiple wavelengths, brain and spinal sections were also analyzed by an Olympus Fluoview microscope, equipped with a BX61 with a confocal FV500 system, at the following four different wavelengths of excitation (laser-channels): 405, 488, 546, and 635 nm. The same evaluation was also extended to the other organs. During the analysis, the following parameters of acquisition (lasers potency, photomultiplier, gain, and offset) were set at the beginning of the analysis (we selected these parameters by the first section corresponding to spinal cord section from the first *mnd* mouse) and then maintained for the whole duration of the study.

Spinal cord and brainstem sections from *mnd* and WT mice were also immunostained with an antibody directed against astrocytes [mouse monoclonal glial fibrillary acidic protein (GFAP) antibody, ImmunologicalScience, Roma,

Italy; dilution 1:1,000] and neurons [mouse anti-NeuN monoclonal antibody, Chemicon Mab 377) (1:1000)], respectively [13]. For both NeuN and GFAP immunofluorescence, the use of a secondary antibody conjugated with a cyanine 5 (peak of excitation at 635 nm) allowed to exclude the possible bias due to the presence of autofluorescent material.

### Electron Microscopy

Four 10-week-old *mnd* mice and the same number of age-matched WT mice were deeply anesthetized and perfused through the ascending aorta with phosphate-buffered saline (PBS, 0.1 M; pH 7.4) solution followed by a 5-min perfusion with 4% paraformaldehyde and 2.5% glutaraldehyde in PBS. Hippocampus was excised and cut in sagittal plane with a razor blade and post-fixed in 3% glutaraldehyde in PBS and then for 2 h in $OsO_4$. After dehydration in graded series of ethanol, tissue samples were cleared in propylene oxide, embedded in Epoxy medium (Epon 812 Fluka), and polymerized at 60°C for 72 h. From each sample, one semithin (1 μm) section was cut with a Leica EM UC6 ultramicrotome and mounted on glass slides for light microscopic inspection to identify the granular layers. Ultrathin (70 nm thick) sections of areas of interest were obtained, counterstained with uranyl acetate and lead citrate, and examined with an energy filter transmission electron microscope (Zeiss Libra® 120) equipped with a YAG scintillator slow scan charge-coupled device camera.

### Blood Preparation

Five 10-week-old *mnd* mice and the same number of age-matched WT mice were killed by decapitation, and blood was collected. Each blood sample was stored in sterile vials pretreated with a solution of 0.25 M EDTA. A volume of 150 μL of blood from each sample was employed for RNA extraction and quantitative real-time PCR (qRT-PCR) analysis. A MiRCURY RNA Isolation Kit-Cell & Plant (Exiqon A/S Skelstedet 16, 2950 Vedbaek, Denmark) was used to extract the total RNA from the blood as indicated in the manufacturer protocol. RNase free water and vials have been used. In order to remove any residual DNA content, a DNase kit (BioLabs) was used. Purity of the total extracted RNA was determined with a Nanodrop ND1000 (Thermo Scientific) by measuring the ratio of absorbance readings at 260 and 280 nm. This ratio was in the range of 1.9–2.1. The extracted samples were stored at −80°C until qRT-PCR.

The remaining collected blood was pooled (one pool of 3 ml per experimental group) and processed with Ficoll Paque TM PLUS for peripheral blood mononuclear cell (PBMC) isolation following the manufacturer protocol. PBMCs were resuspended in sterile PBS containing 1% of BSA and stained on gelatinized slides by cytospin centrifugation (5′ at 20 rpm). Giemsa staining was performed on the spotted cells in order to distinguish nucleated and non-nucleated cells. Bright field images of the treated cells were taken with an Olympus microscope at different magnifications. Epifluorescent (excitation wavelength, 488 nm) images of the same fields were also acquired. The two images were merged in order to correlate the two specific signals.

### Total RNA Preparation

The total RNA samples were prepared from brain, spinal cord, liver, and eyes of 10-week-old *mnd* mice ($n$=5) and the same number of age-matched WT using an Ultra-Turrax homogenizer in the presence of a denaturing guanidium thiocyanate buffer. Purity of the total RNA was determined by the ratio of absorbance readings at 260 and 280 nm; this ratio was in the range of 1.8–2.0. One microgram of total RNA was reverse-transcribed with iScript cDNA Synthesis kit (Bio-Rad, Hercules, CA, USA) to cDNA by a thermal cycler (Applied Instruments, Inc. USA). Glyceraldehyde-3-phosphate dehydrogenase (G3PDH), a housekeeping gene, was used as a control gene to check the consistency of the reverse transcription.

### Quantitative Real-Time PCR

Primers used in the present study were designed by Beacon Designer (BioRad), as shown in Table 1. Quantitative real-time PCR was performed with a SYBR Green kit on the MiniOpticon Two-Color Real-time PCR detection system (Bio-Rad, Milan, Italy). Each PCR reactions including 1 μl of cDNA, 300 nM of each primer, 7.5 μl of mastermix (iQ Sybr Green Supermix, Bio-Rad), and RNase-free water to complete the reaction mixture volume to 15 μl. PCR was performed for 40 cycles at 95°C for 60 s, 58°C annealing temperature for 30 s, and 72°C for 30 s. PCR experiments were performed in triplicate.

The assessment of changes in the gene expression was performed by the method of $2-\Delta\Delta Ct$ normalizing the levels of expression of each target gene compared to housekeeping gene G3PDH. The method $2-\Delta\Delta Ct$ takes for granted that both genes are amplified with an efficiency close to 100% and not <5%.

### Statistical Analysis

The statistical analysis was performed with the Mann–Whitney $U$ test. All data are expressed as mean values ± standard error of mean (SEM). Difference was considered statistically significant if $p<0.05$. Statistics were carried out by using Graph Pad Prism (version 4.0, Graph Pad Software Inc., San Diego, CA, USA).

**Table 1** Primer sequences for use in quantitative real-time RT-PCR assay

| Gene | Primer sequence | Number of base pairs (bp) | Accession number |
|---|---|---|---|
| Glyceraldehyde 3 phosphate dehydrogenase (G3PDH) | F: CTACCCACGGCAAGTTCAAC<br>R: CCAGTAGACTCCACGACATAC | 20<br>21 | NM_008084.2 |
| ATP synthase, lipid-binding protein (ATP synthase) | F: TTCAGACCAGTGTAATCAGCAGAG<br>R: CACCAGAACCAGCAACTCCTAC | 24<br>22 | AF315374 |
| Lysosomal H+/ATPase (H+/ATPase) | F: ATGCTGATGGGTGAAGTGATGAG<br>R: TGGATAACTGTGGTGCTGAAGTC | 23<br>23 | BC063177 |
| Myelin basic protein (isoform 1) (MBP1) | F: GAACACCACCTCCATCCCAAG<br>R: CTGCCTCCGTAGCCAAATCC | 21<br>20 | NM_001025251.2 |
| Myelin basic protein (isoform 2) (MBP2) | F: GGAGCCCTCTGCCCTCTC<br>R: GCCGTGCTGCGACTTCTG | 18<br>18 | NM_001025254.2 |
| Myelin basic protein (isoform 3) (MBP3) | F: CGGGCATCCTTGACTCCATC<br>R: GCCGTGCTGCGACTTCTG | 20<br>18 | NM_001025255.2 |
| Myelin basic protein (isoform 4) (MBP4) | F: GAACACCACCTCCATCCCAAG<br>R: AGATCCAGAGCGGCTGTCTC | 21<br>20 | NM_001025256.2 |
| Myelin basic protein (isoform 5) (MBP5) | F: GGCTCTGGCAAGGACTCAC<br>R: TTGGGATGGAGGTGGTGTTC | 19<br>20 | NM_001025258.2 |

## Results

### *Mnd* Mice Accumulate Lipopigments Early in Different Organs and in Neurons

The analysis of anatomical distribution of autofluorescent material in different organs in 10-week-old *mnd* mice is shown in Fig. 1. In all five animals processed a high accumulation of green fluorescent material was mainly observed in the kidney (Fig. 1a), spleen (Fig. 1b) and lung (Fig. 1c). Although the intracardial perfusion with PBS + Heparin 0.25% avoided any interference due to the circulating cells (blood cells have a high content of lipopigments in NCL patients), it is not possible to exclude that the fluorescence was partially due to the presence of lipopigments in the endothelial cells of vessels (Fig. 1a, b) and/or in the airway layers (Fig. 1c). A lower, but well-detectable fluorescent signal was found in both liver (Fig. 1d) and heart (Fig. 1e) of *mnd* mice but not in the skeletal muscles (Fig. 1f).

The same experiments did not reveal any specific fluorescence in all WT mice analyzed (not shown). These results further supported the reliability of our investigation about

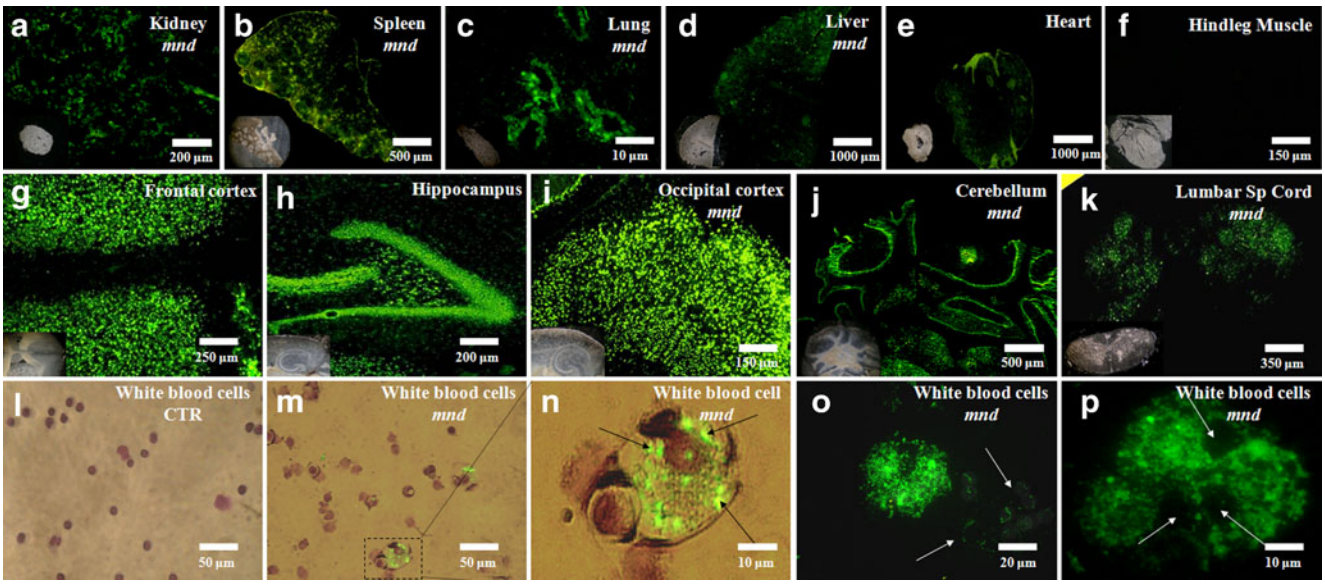


**Fig. 1** Accumulation of autofluorescent material in different organs of 10-week-old *mnd* mouse females. **a**–**f** Peripheral organs. **g**–**k** Central nervous system. **l**–**p** White blood cells (**l** and **m** were obtained by overlapping the images in dark field after Giemsa staining and the fluorescence images with an excitation laser at 488 nm)

the lipopigment accumulation in peripheral tissues of *mnd* mice.

The examination carried out in CNS confirmed the very high accumulation of autofluorescent material with various degree of fluorescent signal in many regions of the CNS. In particular, the presence of a massive accumulation of fluorescent material was observed in the neuronal layer in the frontal cortex (Fig. 1g), in different CAs regions and in the dentate gyrus of the hippocampus (Fig. 1h), in the cortical layers of the occipital brain region (Fig. 1i), and in the cerebellar cortex and in the deep nuclei of the cerebellum (Fig. 1j) and in the whole length of spinal cord (Fig. 1k).

The possible accumulation of autofluorescent pigments was also analyzed in peripheral blood cells (leukocytes) from both *mnd* and healthy mice. As expected, the merge between the Giemsa staining (purple cells) and the excitation to 488 nm did not show the presence of autofluorescent material in blood cells from 10-week-old WT mice (Fig. 1l). In contrast, the same procedure of fluorescence visualization clearly showed the presence of a high content of autofluorescent material in blood cells with a large cytoplasm (megakaricytes or macrophages presumably) (Fig. 1m). High magnification picture (Fig. 1n) further confirmed the segregation of green-fluorescent spots into the cytoplasm; no evidence of green-stained spots was found in nuclei (purple staining).

The visualization of white blood cells from *mnd* mice (Fig. 1o, p) furthermore confirmed the punctuate pattern of autofluorescence in large-sized cells and also revealed the presence of smaller cells with (Fig. 1o, white arrows) milder, but detectable signal fluorescent spots around the nuclei (dark circles). Higher magnified picture (Fig. 1p) allows to visualize in more detail the lack of autofluorescent signal in the nucleus (see arrows) of white blood cells.

The excitation of spinal cord with lasers from 405 to 635 nm confirmed that stored material is detectable at different wavelengths (Fig. 2a). However, this experiments also revealed that the maximal peak of excitation is around 450–550 nm, which rapidly disappears beyond 600 nm (infrared channel). The punctuate green staining observed in white blood cells was also observed in neurons. Representative high magnification pictures from spinal motor neurons of *mnd* mouse (Fig. 2b) confirmed the not selective excitation of storage material and also showed the punctuate storage of autofluorescent material. The colocalization between the immunostaining with the pan-neuronal marker NeuN (Fig. 2d) and the autofluorescence associated with lipopigment accumulation (Fig. 2c) in the brainstem (as in other brain regions) showed a high degree of overlapping between the two signals (Fig. 2e). On the other hand, the merging of the immunostaining with a marker of active astrocytes, the GFAP (Fig. 2g), and the green signal from the excitation of autofluorescent material (Fig. 2f) did not reveal any colocalization between astrocytes and lipofuscin (Fig. 2h). As expected, a complete lack of autofluorescent material deposition was found in CNS or other tissues from 10-week-old WT mice (not shown).

Ultrastructural evaluation by electron microscopy showed nucleus and cytoplasmic organelles with their characteristic morphology in a granule cell of hippocampus from WT mice (Fig. 3a). Abnormal accumulation of lipofuscin granules was observed in the cytoplasm of hippocampal granule cells of *mnd* mice (Fig. 3b). Furthermore, at higher magnification, it is possible to appreciate the complex aggregation of lipofuscin granules and the degeneration processes of varying severity in mitochondria, leading in some cases to complete disruption of internal components (Fig. 3c) or limited to some areas of the inner membrane (Fig. 3d).

## Lipofuscin Accumulation is Associated with Important Changes in the Gene Expression

Lipofuscin accumulation is associated with important changes in the gene expression of the three following genes: (1) ATP synthase lipid-binding protein, subunit c; (2) lysosomal $H^+$/ATPase, V1 subunit D; and (3) MBP.

The modulation of gene expression of ATP synthase lipid-binding protein in the *mnd* mouse versus WT in spinal cord, brain, liver, and eyes has been expressed in Fig. 4, where the graphs show the modulation of gene expression in *mnd* mice compared to WT as estimated by the $\Delta\Delta C_t$ method. We can observe a large increase in the expression of ATP synthase in the *mnd* mice spinal cord compared to WT. The increase remains even in the brain as well as in the liver, although to a lesser extent. An increase in ATP synthase lipid-binding protein gene expression is also present in the blood of *mnd* mice compared to WT (Fig. 7a). Otherwise, in eyes, the expression of ATP synthase is statistically significantly decreased in *mnd* mice compared to WT.

The modulation of gene expression of lysosomal $H^+$/ATPase ($H^+$/ATP) in the *mnd* mouse versus WT in spinal cord, brain, liver, and eyes has been shown in Fig. 5. A statistically significant increase in gene expression for the lysosomal $H^+$/ATPase has been observed in the liver, while in the brain and in the spinal cord, the lysosomal $H^+$/ATPase is modulated in a statistically significant but less extensive way than that observed in the liver. In the eyes, a statistically significant decrease in ATP lipid-binding protein expression was observed in *mnd* mice compared to WT.

The modulation of gene expression of MBP in the *mnd* mouse versus WT in spinal cord, brain, liver, and eyes has been synthesized in Fig. 6. In particular, five different isoforms of MBP have been described in mice. A strong increase in the expression of almost all MBP isoforms has been observed in the liver (except isoform 5), while in the

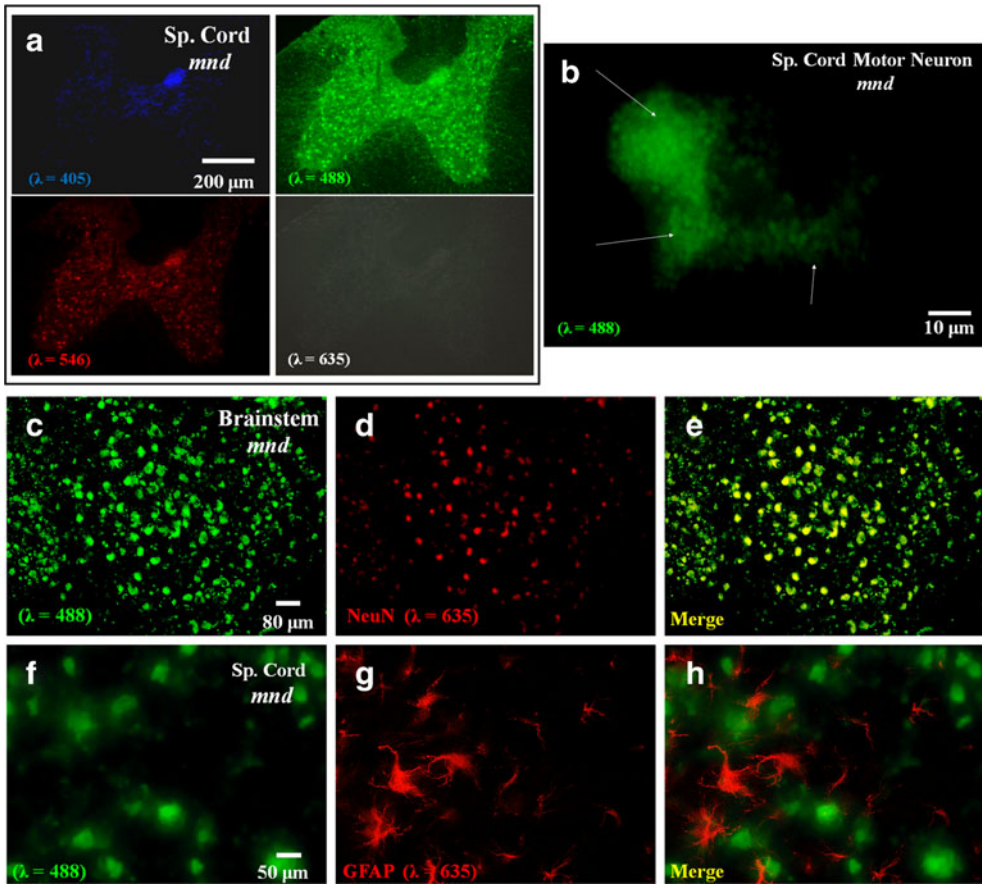


**Fig. 2** Representative pattern of autofluorescence at the spinal cord level in 10-week-old *mnd* mouse at excited by four different length waves λ (**a**). To perform a comparative analysis all parameters of acquisition (setting of laser potency, photomultipliers, gain, and offset) were kept for each laser utilized. In addition, since the stability of natural pigments to the laser scanning is very low in comparison with commercial dyes, we also randomized the order of scanning for each single laser. No appreciable difference was observed by modifying the order of scanning. High magnified picture showing the punctuate staining associated with autofluorescent spots into the cytoplasm of spinal cord motor neuron from a 10-week-old *mnd* mouse (**b**). Immunofluorescence experiments between NeuN positive neurons (**d**) and autofluorescent material (**c**) revealed an almost complete co-localization between the two signals (**e**). The merge between autofluorescent material (**f**) and GFAP positive astrocytes (**g**) did not show colocalization between the two signals (**h**). No presence of lipopigment-related signal was observed in adjacent slides of those processed for immunohistochemical studies when excited to 635 nm

spinal cord, an increase in the isoforms 1 and 2 is resulted statistically significantly. In the brain, an increase in MBP isoform 1 has been observed, while the modulation of all other isoforms was not statistically significant in *mnd* mice compared to WT. In the eyes, no significant change of MBP isoform expression in *mnd* mice compared to WT has been observed.

Finally, the results show that, in *mnd* mice, both lysosomal H+/ATPase and MBP expression slightly increased, but the data are not statistically significant (Fig 7b, c).

## Discussion

The present data show that: (1) a differential expression of lysosomal $H^+$/ATPase, V1 subunit D gene, and ATP synthase lipid-binding protein, subunit c gene occurs in *mnd* with reference to age-matched WT mice; (2) some isoforms of MBP are overexpressed in the brain, spinal cord, and liver but not in the eyes or in the blood cells of *mnd* mice; and (3) ATP synthase lipid-binding protein is selectively increased in the blood of *mnd* mice. This finding makes it as an important candidate for the validation of peripheral biomarkers in *cln8* gene mutation-related disorders. The presence of these changes in peripheral areas and in CNS of mice several weeks before symptoms appearance suggests that modifications in gene transcription may be somehow associated with lipopigment accumulation rather than being a downstream event of pathological alterations.

In particular, lysosomal $H^+$/ATPase, V1 subunit D gene and ATP synthase lipid-binding protein, subunit c gene were mainly expressed in the brain, spinal cord, and liver of *mnd* mice, with respect to wild type; in contrast, the same genes were less expressed in the eyes of *mnd* model mice with

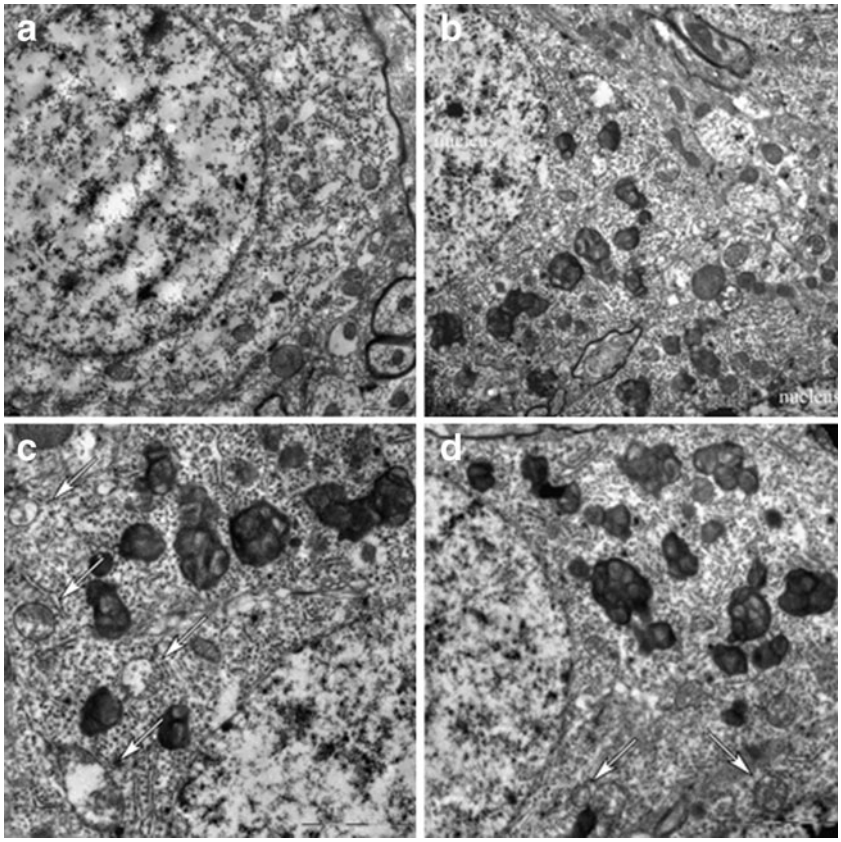


**Fig. 3** Ultrastructure analysis of hippocampal granular layer by transmission electron microscopy of WT (**a**) and mnd (**b**) mice. In **b**, accumulation of electron dense lipofuscin granules is observed in the cytoplasm of two adjacent granule cells with nuclei visible at the *upper left and bottom right corner*. Transmission electron micrographs at higher magnification depicted the aggregation of lipofuscin granules and complete (**c**) or partial disruption (**d**) of inner membranes of mitochondria (*white arrows*)

respect to wild type. Since the eye is composed of different tissues, such as the lens, retina, and sclera, it is possible that we observed a combination of different effects on various tissues. The subunit c of mitochondrial ATP synthase is the major protein accumulated in the storage bodies of animals or humans affected by NCL and also in the *mnd* mice model probably due to an increase of ATP-synthase lipid-binding protein gene expression [14]. In addition, in *mnd* mice increased expression of the lysosomal $H^+$ pump gene suggests a compensatory mechanism of the abnormal lysosomal pH, and the increased $H^+$/ATPase might rebalance the pH homeostasis within the cell and normalize the pool of enzymes [11].

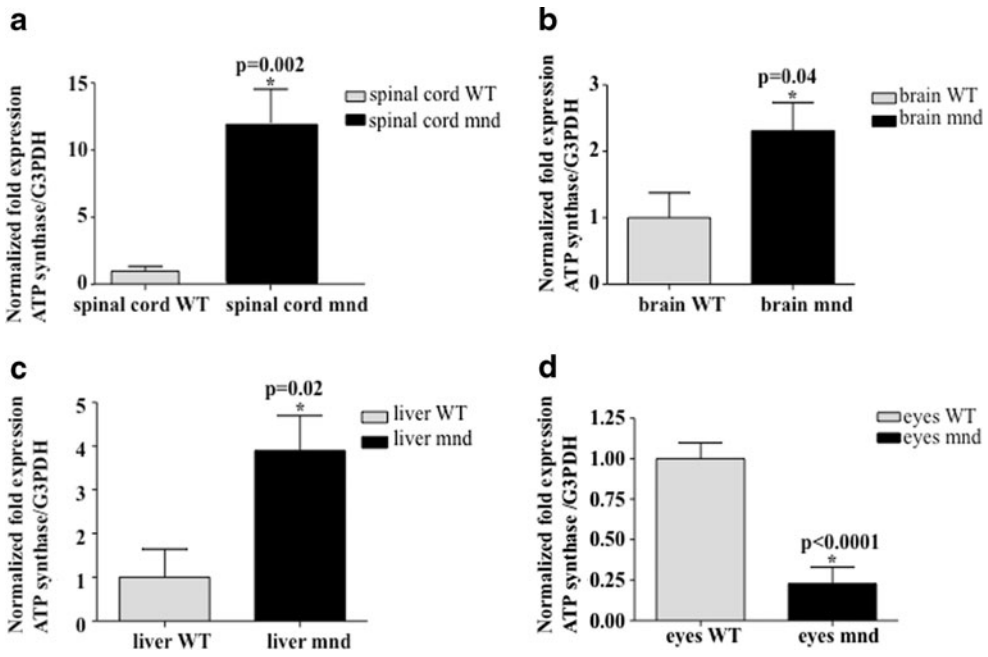


**Fig. 4** Gene expression of ATP synthase lipid-binding protein (ATP synthase) in the *mnd* mouse vs WT is presented. **a** Increased expression of the *mnd* mouse vs WT (WT 1.000±0.815, *mnd* 12.304±5.573; $n=5$; $p=0.002$) in the spinal cord. (**b**) Increased expression in the *mnd* mouse vs WT (WT 1.000±0.380, *mnd* 2.312±0.421; $n=5$; $p=0.04$) in the brain. **c** Increased expression of the *mnd* mouse vs WT (WT 1.000±0.650, *mnd* 3.901±0.800; $n=5$; $p=0.02$) in the liver. **d** Reduced expression in the *mnd* vs WT (WT 1.000±0.09, *mnd* 0.230±0.10; $n=5$; $p<0.0001$) in the eyes

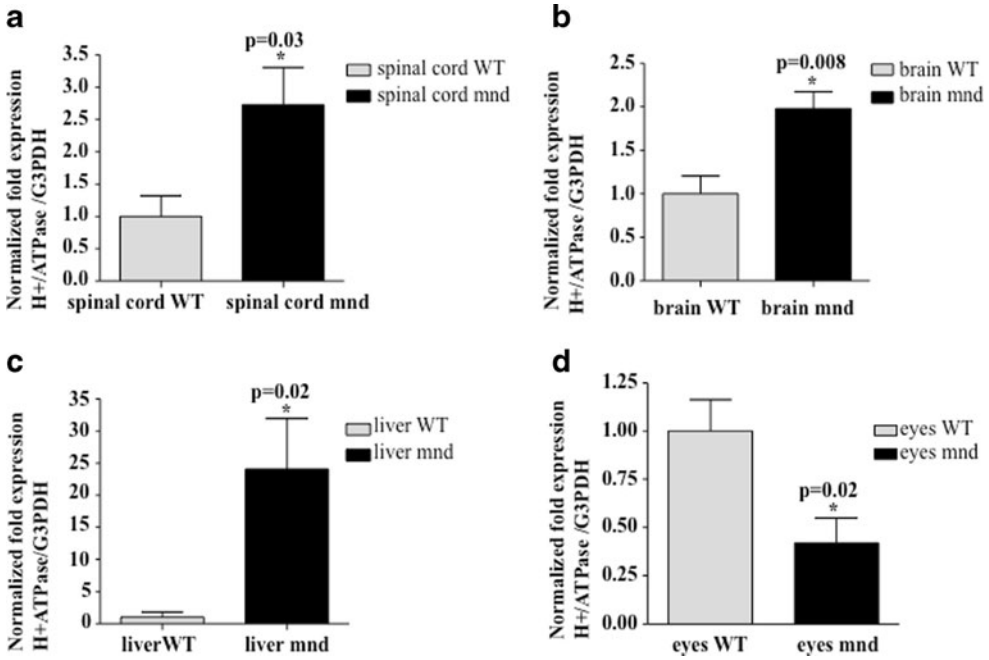


**Fig. 5** Gene expression of Lysosomal H+/ATPase (H+/ATPase) in the *mnd* mouse vs WT is presented. **a** Increased expression of the *mnd* mouse vs WT (WT 1.000±0.710, *mnd* 2.728±1.283; $n=5$; $p=0.03$) in the spinal cord. **b** Increased expression in the *mnd* mouse vs WT (WT 1.000±0.464, *mnd* 1.979±0.438; $n=5$; $p=0.008$) in the brain. **c** Increased expression of the *mnd* mouse vs WT (WT 1.000±0.820, *mnd* 24.11±7.856; $n=5$; $p=0.02$) in the liver. **d** Lower expression in the *mnd* vs WT (WT 1.000±0.163, *mnd* 0.420±0.130; $n=5$; $p=0.02$) in the eyes

Previous studies reported that ATP synthase lipid-binding protein, subunit c, initially located in the mitochondria, accumulated in the lysosomes of NCL cells. This event suggests that the intracellular trafficking of specific molecules to the lysosome, where the degradative process occurs, is severely altered [15, 16]. Hence, an impairment of lysosomal pH homeostasis might be the pivotal mechanism by which the lysosomal storage disorder arises. A loss of $H^+$/ATPases results in a marked accumulation of the subunit c of mitochondrial ATP synthase and increased amounts of lysosomal enzymes [17]. In addition, our results demonstrated an increase in gene expression of certain MBP isoforms in various tissues. In particular, we highlighted that, in the brain, there is an increase in isoform 1 expression; whereas in the spinal cord, isoforms 1 and 2 were increased; in the liver, isoforms 1–4 are potentiated; and in the eyes, no changes in isoform expression were observed. In addition, our data show that, in *mnd* mice, both lysosomal $H^+$/ATPase and MBP expression increased slightly, but not sufficiently to reach statistical significance. This result might be due to the presence in the blood of various cell types differing in gene expression. Further studies will clarify these results. On the other hand, the significant increase in the expression of ATP synthase lipid-binding protein in both peripheral and nervous tissue strongly suggests the presence of a new common marker associated with *cln8* mutation. This could be of extreme relevance for future studies aimed at evaluating differences between peripheral and central levels at various phases of neurological clinical progression or upon systemic treatment in *mnd* mice. In this context, modulation of these genes in both peripheral and central tissues with ALC will be of particular interest for two main reasons: (1) it was shown that ALC modulates the expression of this genes in basal conditions [11], and (2) the chronic treatment with ALC significantly reduced the clinical progression of *mnd* mice by restoring the mitochondrial functionality [8].

The changes in gene expression either in liver or brain regions are accompanied by a similar increase in autofluorescent material in both organs. The accumulation of autofluorescent lipopigment granules in liver, cardiomyocytes, skeletal muscle, skin and endocrine glands has already been reported in autosomal dominant adult neuronal ceroid lipofuscinosis [18]. However, it is important to underline that lipopigment accumulation from the livers of sheep affected with ceroid lipofuscinosis showed that the disease does not involve a defect in lipid metabolism or abnormal lipid peroxidation and that most of them were proteinaceous [19]. These data reinforces the hypothesis that the process of accumulation in the liver is similar to those involving neurons and peripheral cells in different forms of lysosomal storage disorders (LSDs) [20, 21].

MBP is a fundamental component of myelin, which is a dynamic structure arising from oligodendrocyte membrane processes during the myelination of nerve fibers. Genes of oligodendrocytes lineage give rise to different developmentally regulated splice isoform of MBP. In rodents, four isoforms of MBP gene expression resulting from alternative splicing of the gene Golli have been identified [22]. The MBP isoforms differ in their molecular weight: the most abundant in the CNS of rodents are the L isoform (14 kDa) and S isoform (18 kDa), which, together, represent the majority of MBP present in myelin. In cultured rat neurons, it has been shown that the MBP isoforms containing exon II, the 21.5 and 17 kDa isoforms, were distributed diffusely in

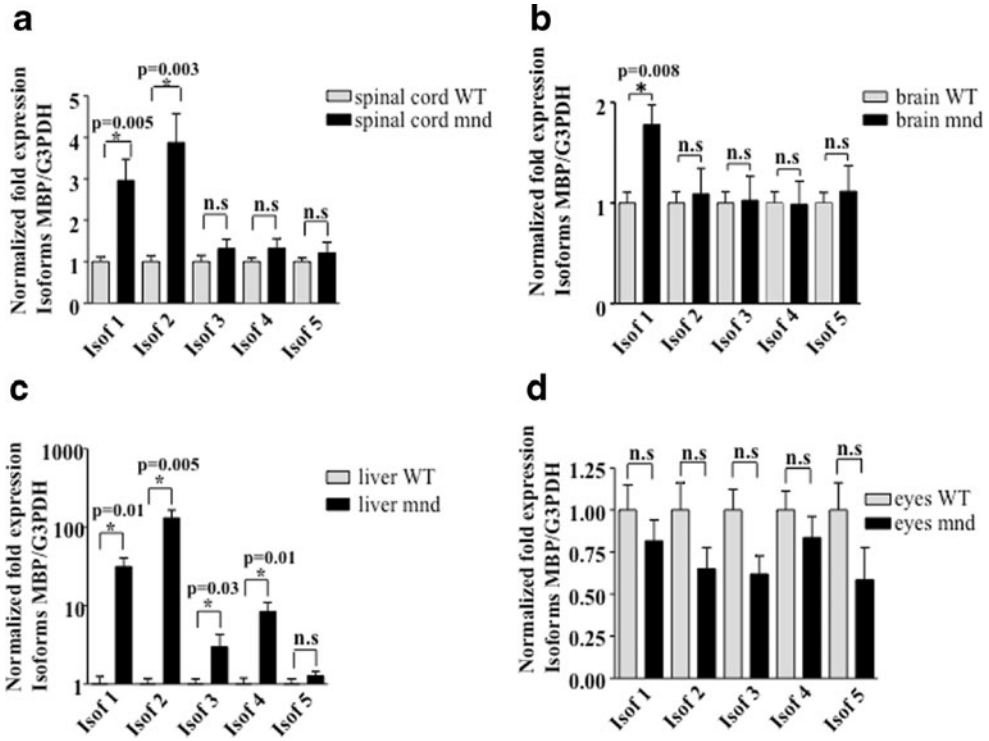


**Fig. 6** The figure shows the gene expression of MBP in the *mnd* mouse vs WT. **a** Increased expression of 1 and 2 isoforms in the *mnd* mouse vs WT, whereas isoforms 3–5 are not statistically significant (Isof1) WT 1.000±0.270, *mnd* 2.963±1.146, n=5; p=0.005; (Isof2) WT 1.000±0.334, *mnd* 3.883, ± 1.552, *n*=5; *p*=0.003; (Isof3) WT 1.000±0.342, *mnd* 1.314±0.511, *n*=5; *p*=n.s; (Isof4) WT 1.000± 0.210, *mnd* 1.329±0.505, *n*=5; *p*=n.s; (Isof5) WT 1.000±0.203, *mnd* 1.209±0.457, *n*=5; *p*=n.s) in the spinal cord. **b** Increased expression in isoform 1 in the *mnd* mouse vs WT; the other isoforms are not statistically significant (Isof1) WT 1.000±0.241, *mnd* 1.781±0.436, *n*=5 ; *p*=0.008 (Isof2) WT 1.000±0.253, *mnd* 1.091, ± 0.568, *n*=5; *p*= n.s; (Isof3) WT 1.000±0.254, *mnd* 1.027±0.542, *n*=5; *p*=n.s; (Isof4) WT 1.000±0.256, *mnd* 1.010±0.519, *n*=5; *p*=n.s; (Isof5) WT 1.000± 0.232, *mnd* 1.117±0.572, *n*=5; *p*=n.s) in the brain. **c** Increased expression of the *mnd* mouse vs WT in both isoform 1 and 2, <3.4, while in the isoform 5, it is not statistically significant (Isof1) WT 1.000±0.572, *mnd* 31.591±20.698, *n*=5; *p*=0.01; (Isof2) WT 1.000± 0.393, *mnd* 131.122, ±77.557, *n*=5; *p*=0.005; (Isof3) WT 1.000± 0.370, *mnd* 3.000±2.902, *n*=5; *p*=0.003; (Isof4) WT 1.000±0.420, *mnd* 8.445±5.670, *n*=5; *p*=0.001; (Isof5) WT 1.000±0.382, *mnd* 1.279±0.384, *n*=5; *p*=n.s) in the liver. **d** Reduced expression that not statistically significant in all isoforms in the *mnd* mouse vs WT (Isof1) WT 1.000±0.148, *mnd* 0.816±0.126, *n*=5; *p*=n.s; (Isof2) WT 1.000±0.153, *mnd* 0.652, ±0.122, *n*=5; *p*=n.s; (Isof3) WT 1.000± 0.123, *mnd* 0.619±0.108, *n*=5; *p*=n.s; (Isof4) WT 1.000±0.113, *mnd* 0.836±0.126, *n*=5; *p*=n.s; (Isof5) WT 1.000±0.161, *mnd* 0.586± 0.188, *n*=5; *p*=n.s in the eyes

the cytoplasm and accumulated in the nucleus only during the process of maturation of oligodendrocytes, which plays a key regulatory role in initiating myelinogenesis. In contrast, L and S isoforms, lacking exon II, play an essential role in the compact myelin sheath. The classical isoforms of MBP include the 18.5 kDa form, which prevails in adult human myelin and facilitates compaction of the mature myelin sheath in the central nervous system, thereby maintaining its structural integrity. The 18.5 kDa and all other classic isoforms are able to interact with a number of proteins, including $Ca^{2+}$-calmodulin, actin, tubulin, and SH3-domain containing proteins, and thus, they may represent signaling linkers during myelin development and remodeling.

Many studies have shown that these MBP proteins are able to activate a strong immune response leading to a chronic disease characterized by myelin loss and excessive levels of MBP in cerebrospinal fluid of patients with multiple sclerosis (MS) [23, 24]. MBP in cerebrospinal fluid is an indicator of disease activity in MS. In addition, patients with neurometabolic diseases exhibit a MBP increase in the blood [25].

Although lipofuscin accumulated in almost all neuronal (and non-neuronal) cells in both NCLs patients and animal models, few results have been reported regarding the possible correlation between the progressive accumulation of autofluorescent materials and cell dysfunction in *mnd* mice. Early accumulation of lipopigment has been reported in the cortex and hippocampus, with the loss of a subpopulation of GABAergic interneurons [26]. Thus, the accumulation of undigested material may somehow have reduced the efficiency of inhibitory neurons, thereby leading to neuronal hyperactivity and seizure susceptibility as recently shown by our group [27]. In line with these results, glutamtergic unbalance and excitatory overstimulation have been also demonstrated in the spinal cord region of *mnd* mice [28],

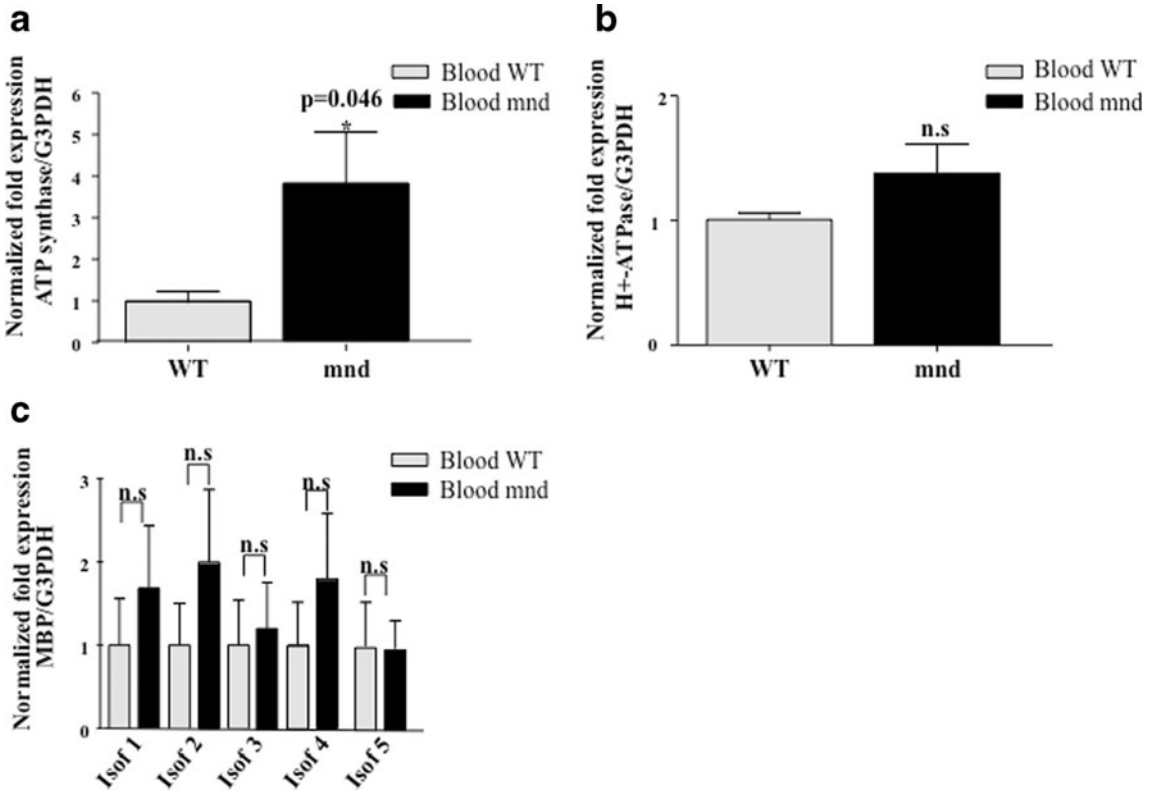


**Fig. 7** Gene expression of ATP synthase lipid-binding protein (**a**), H+/ATPase (**b**), and MBP isoforms (**c**) in the blood. **a** Statistically significant increased expression of ATP synthase gene of the *mnd* mouse vs WT (WT 1.000±0.276, *mnd* 3.783±1.309, $n$=5, $p$=0.0468); **b** WT 1.000±0.054, *mnd* 1.360±0.231, $n$=5, $p$=0.124, no statistically significance; **c** (Iso1) WT 1.000±0.561, *mnd* 1.686±0.750, $n$=5, $p$=0.470; (Iso2) WT 1.000±0.505, *mnd* 1.998±0.873, $n$=5, $p$=0.330; (Iso3) WT 1.000±0.542, *mnd* 1.221±0.555, $n$=5, $p$=0.777; (Iso4) WT 1.000±0.528, *mnd* 1.799±0.784, $n$=5, $p$=0.405; (Iso5) WT 1.000±0.534, *mnd* 0.974±0.335, $n$=5, $p$=0.967, not statistically significant in all isoforms

and it has also been reported that the chronic treatment with glutamatergic antagonists [29, 30] further strengthens this hypothesis. The histological characterization showed in the present study confirmed the marked and spread distribution of autofluorescent material in the brain and spinal cord of young animals. We found that the early accumulation of autofluorescent material both involves cerebral and peripheral tissues and seems to influence the transcription of important genes independently of the anatomical site and the pathological condition. The drastic reduction in mRNA levels from the ocular samples of *mnd* mice is very interesting and seems to further suggest the link between lipofuscin accumulation and the transcription of these genes. We have previously described that, in contrast to other organs, retinal layer cells accumulate lipofuscin in very early phases of postnatal dye and rapidly degenerate and disappear [5]. We also reported that this process is more accelerated in females, where an almost complete degeneration of affected cells occurs from the sixth to the eighth week of life.

The lack of autofluorescent material deposition in activated astrocytes was first found in different brain areas of 10-week-old *mnd* mice: It does not reduce the role of reactive gliosis in enhancing the progression of the symptoms in NCL patients. In this context, the recent discovery achieved from a murine model of infantile neuronal ceroid lipofuscinosis, indicating an early stage reactive gliosis and a primary pathology in astrocytes, including changes in S100beta and GLAST expression [31], seems to confirm our previous studies in the spinal cord and hippocampus of *mnd* mice [27, 28]. Since MBP proteins are able to activate a strong immune response, it is possible to hypothesize a link between the changes in MBP mRNA levels and a further increase in glial activation and neuroinflammation in the brain regions of *mnd* mice.

This study potentially represents an important step towards the identification of biomarkers associated with lipopigment accumulation in NCLs, not exclusively related to the affected areas, but also extendible to peripheral tissues. In this context, the presence of lipopigments in NCLs patients [32] may be a useful starting point to measure alterations of gene expression at the clinical level, and the large series of studies in different types of LSDs at preclinical [33] and clinical levels [20, 34] seem to validate this idea of a possible diagnostic approach.

**Acknowledgments** Authors are very grateful to Dr. Katia Paolella for her technical help. The authors thank Dr. James Neil Fisher for help with manuscript editing.

## References


1. Mole SE, Williams RE, Goebel HH (2005) Correlations between genotype, ultrastructural morphology and clinical phenotype in the neuronal ceroid lipofuscinoses. Neurogenetics 6:107–126
2. Haltia M (2003) The neuronal ceroid-lipofuscinoses. J Neuropathol Exp Neurol 62:1–13
3. Ranta S, Zhang Y, Ross B et al (1999) The neuronal ceroid lipofuscinoses in human EPMR and mnd mutant mice are associated with mutations in CLN8. Nat Genet 23:233–236
4. Messer A, Plummer J, Wong V, Lavail MM (1993) Retinal degeneration in motor neuron degeneration (mnd) mutant mice. Exp Eye Res 57:637–641
5. Guarneri R, Russo D, Cascio C et al (2004) Retinal oxidation, apoptosis and age- and sex-differences in the mnd mutant mouse, a model of neuronal ceroid lipofuscinosis. Brain Res 1014:209–220
6. Messer A, Plummer J (1993) Accumulating autofluorescent material as a marker for early changes in the spinal cord of the Mnd mouse. Neuromuscul Disord 3:129–134
7. Pardo CA, Rabin BA, Palmer DN, Price DL (1994) Accumulation of the adenosine triphosphate synthase subunit C in the mnd mutant mouse. A model for neuronal ceroid lipofuscinosis. Am J Pathol 144:829–835
8. Bertamini M, Marzani B, Guarneri R et al (2002) Mitochondrial oxidative metabolism in motor neuron degeneration (mnd) mouse central nervous system. Eur J Neurosci 16:2291–2296
9. Traina G, Federighi G, Macchi M, Bernardi R, Durante M, Brunelli M (2011) Modulation of myelin basic protein gene expression by acetyl-L -carnitine. Mol Neurobiol 44:1–6
10. Traina G, Valleggi S, Bernardi R et al (2004) Identification of differentially expressed genes induced in the rat brain by acetyl-L-carnitine as evidenced by suppression subtractive hybridisation. Brain Res Mol Brain Res 132:57–63
11. Traina G, Bernardi R, Cataldo E, Macchi M, Durante M, Brunelli M (2008) In the rat brain acetyl-L-carnitine treatment modulates the expression of genes involved in neuronal ceroid lipofuscinosis. Mol Neurobiol 38:146–152
12. Bigini P, Mennini T (2004) Immunohistochemical localization of TNFalpha and its receptors in the rodent central nervous system. Methods Mol Med 98:73–80
13. Mennini T, Bigini P, Cagnotto A et al (2004) Glial activation and TNFR-I upregulation precedes motor dysfunction in the spinal cord of mnd mice. Cytokine 25:127–135
14. Faust JR, Rodman JS, Daniel PF, Dice JF, Bronson RT (1994) Two related proteolipids and dolichol-linked oligosaccharides accumulate in motor neuron degeneration mice (mnd/mnd), a model for neuronal ceroid lipofuscinosis. J Biol Chem 269:10150–10155
15. Sun-Wada GH, Wada Y, Futai M (2003) Lysosome and lysosome-related organelles responsible for specialized functions in higher organisms, with special emphasis on vacuolar-type proton ATPase. Cell Struct Funct 28:455–463
16. Sun-Wada GH, Wada Y, Futai M (2003) Vacuolar H+pumping ATPases in luminal acidic organelles and extracellular compartments: common rotational mechanism and diverse physiological roles. J Bioenerg Biomembr 35:347–358
17. Kasper D, Planells-Cases R, Fuhrmann JC et al (2005) Loss of the chloride channel ClC-7 leads to lysosomal storage disease and neurodegeneration. EMBO J 24:1079–1091
18. Nijssen PC, Ceuterick C, van Diggelen OP et al (2003) Autosomal dominant adult neuronal ceroid lipofuscinosis: a novel form of NCL with granular osmiophilic deposits without palmitoyl protein thioesterase 1 deficiency. Brain Pathol 13:574–581
19. Palmer DN, Barns G, Husbands DR, Jolly RD (1986) Ceroid lipofuscinosis in sheep. II. The major component of the lipopigment in liver, kidney, pancreas, and brain is low molecular weight protein. J Biol Chem 261:1773–1777
20. Boriack RL, Cortinas E, Bennett MJ (1995) Mitochondrial damage results in a reversible increase in lysosomal storage material in lymphoblasts from patients with juvenile neuronal ceroid-lipofuscinosis (Batten Disease). Am J Med Genet 57:301–303
21. Woloszynek JC, Coleman T, Semenkovich CF, Sands MS (2007) Lysosomal dysfunction results in altered energy balance. J Biol Chem 282:35765–35771
22. Baumann N, Pham-Dinh D (2001) Biology of oligodendrocyte and myelin in the mammalian central nervous system. Physiol Rev 81:871–927
23. Quarles RH (1997) Glycoproteins of myelin sheaths. J Mol Neurosci 8:1–12
24. Tansey FA, Farooq M, Cammer W (1991) Glutamine synthetase in oligodendrocytes and astrocytes: new biochemical and immunocytochemical evidence. J Neurochem 56:266–272
25. Lamers KJ, Vos P, Verbeek MM, Rosmalen F, van Geel WJ, van Engelen BG (2003) Protein S-100B, neuron-specific enolase (NSE), myelin basic protein (MBP) and glial fibrillary acidic protein (GFAP) in cerebrospinal fluid (CSF) and blood of neurological patients. Brain Res Bull 61:261–264
26. Cooper JD, Messer A, Feng AK, Chua-Couzens J, Mobley WC (1999) Apparent loss and hypertrophy of interneurons in a mouse model of neuronal ceroid lipofuscinosis: evidence for partial response to insulin-like growth factor-1 treatment. J Neurosci 19:2556–2567
27. Melo T, Bigini P, Sonnewald U et al (2010) Neuronal hyperexcitability and seizures are associated with changes in glial-neuronal interactions in the hippocampus of a mouse model of epilepsy with mental retardation. J Neurochem 115(6):1445–1454
28. Mennini T, Bigini P, Ravizza T et al (2002) Expression of glutamate receptor subtypes in the spinal cord of control and mnd mice, a model of motor neuron disorder. J Neurosci Res 70:553–560
29. Elger B, Schneider M, Winter E et al (2006) Optimized synthesis of AMPA receptor antagonist ZK 187638 and neurobehavioral activity in a mouse model of neuronal ceroid lipofuscinosis. ChemMedChem 1:1142–1148
30. Mennini T, Cagnotto A, Carvelli L et al (1999) Biochemical and pharmacological evidence of a functional role of AMPA receptors in motor neuron dysfunction in mnd mice. Eur J Neurosci 11:1705–1710
31. Macauley SL, Wozniak DF, Kielar C, Tan Y, Cooper JD, Sands MS (2009) Cerebellar pathology and motor deficits in the palmitoyl protein thioesterase 1-deficient mouse. Exp Neurol 217:124–135
32. Williams RE, Aberg L, Autti T, Goebel HH, Kohlschutter A, Lonnqvist T (2006) Diagnosis of the neuronal ceroid lipofuscinoses: an update. Biochim Biophys Acta 1762:865–872
33. Reolon GK, Reinke A, de Oliveira MR et al (2009) Alterations in oxidative markers in the cerebellum and peripheral organs in MPS I mice. Cell Mol Neurobiol 29:443–448
34. Manca V, Kanitakis J, Zambruno G, Thivolet J, Gonnaud PM (1990) Ultrastructural study of the skin in a case of juvenile ceroid-lipofuscinosis. Am J Dermatopathol 12:412–416